The Astrophysical Journal Letters, 886:L26 (4pp), 2019 December 1 https://doi.org/10.3847/2041-8213/ab563f

Particle Acceleration in Shearing Flows: Efficiencies and Limits

Frank M. Rieger[1,2] and Peter Duffy[3]
[1] ZAH, Institute of Theoretical Astrophysics, University of Heidelberg, Philosophenweg 12, D-69120 Heidelberg, Germany; f.rieger@uni-heidelberg.de
[2] Max-Planck-Institut für Kernphysik, Saupfercheckweg 1, D-69117 Heidelberg, Germany
[3] School of Physics, University College Dublin, Belfield, Dublin 4, Ireland
Received 2019 October 23; revised 2019 November 8; accepted 2019 November 9; published 2019 November 22

Abstract

We examine limits to the efficiency for particle acceleration in shearing flows, showing that relativistic flow speeds are required for efficient gradual shear acceleration. We estimate maximum achievable particle energies for parameters applicable to the relativistic jets of active galactic nuclei. The implications of our estimates is that if large-scale jets are relativistic, then efficient electron acceleration up to several PeV and proton acceleration up to several EeV energies appears feasible. This suggests that shear particle acceleration could lead to a continued energization of synchrotron X-ray emitting electrons, and be of relevance for the production of ultra-high-energy cosmic-ray particles.

Unified Astronomy Thesaurus concepts: Radio jets (1347); Relativistic jets (1390); Ultra-high-energy cosmic radiation (1733); High energy astrophysics (739)

1. Introduction

Shear flows are expected to be present in various astrophysical environments. Prototypical examples include black hole accretion flows and the relativistic outflows or jets in gamma-ray bursts and active galactic nuclei (AGN; Rieger & Duffy 2004). The jets in AGN, for example, are likely to exhibit some internal velocity stratification from the outset, shaped by a highly relativistic, ergo-spheric driven (electron–positron) flow that is surrounded by a slower moving (electron–proton dominated) wind from the inner parts of the disk (e.g., Fendt 2019; Martí 2019 and references therein). As these jets propagate, interactions with the ambient medium is know to excite instabilities and to induce mass loading, enforcing further velocity shearing (e.g., Perucho 2019 and references therein). Radio images of parcec-scale jets in AGN indeed provide phenomenological evidence for internal jet stratification, examples including limb-brightened structures or boundary layers with parallel magnetic fields (e.g., Giroletti et al. 2008; Blasi et al. 2013; Gabuzda et al. 2014; Nagai et al. 2014; Piner & Edwards 2014; Boccardi et al. 2016). When taken together, this suggests that transversal velocity stratification and shear is a generic feature of AGN-type jets. Given the diversity of observed emission properties, this has in recent times generated new interest in multi-zone or spine-shear-layer acceleration and emission models (e.g., Sahayanathan 2009; Laing & Bridle 2014; Tavecchio & Ghisellini 2015; Rieger & Duffy 2016; Chhotray et al. 2017; Liang et al. 2017; Liu et al. 2017; Kimura et al. 2018; Webb et al. 2018).

Shear flows can in principle facilitate particle acceleration by several means (see Rieger 2019 for a recent review). One prominent possibility includes a stochastic Fermi-type mechanism, in which particle energization occurs as a result of elastically scattering off differentially moving (magnetic) inhomogeneities (e.g., Berezhko & Krymskii 1981; Earl et al. 1988; Webb 1989; Rieger & Duffy 2006; Lemoine 2019). In gradual shear particle acceleration these inhomogeneities are considered to be frozen into a background flow whose bulk velocity varies smoothly in the transverse direction. The scattering center's speeds are thus essentially characterized by the general bulk flow profile. Given recent developments, this Letter studies the requirements for this mechanism to operate efficiently and discusses the resultant limits on the achievable maximum energies when applied to AGN-type jets.

2. Particle Spectra

As a stochastic particle acceleration process, the space-independent part of gradual shear acceleration obeys a diffusion equation in momentum space (e.g., Earl et al. 1988; Rieger & Duffy 2006). While moving across the velocity shear the particle momentum relative to the flow changes, so that in the local scattering frame a net increase in momentum can occur. Hence, particle acceleration is closely tied to the diffusive transport across the flow. This, however, also implies that particles can diffusively escape from the system, impacting on the shapes of possible particle spectra. This becomes particularly relevant for non-relativistic flow speeds where cross-field escape counterbalances efficient particle acceleration. When diffusive escape and radiative losses are neglected, non-relativistic gradual shear acceleration is known to lead to power-law particle spectra $n(p) \propto p^2 f(p) \propto p^{-(1+\alpha)}$ for an energetic particle diffusion coefficient scaling as $\kappa \propto p^{\alpha}$ (Berezhko 1982; Rieger & Duffy 2006). With reference to an analytical steady-state model based on the full particle transport equation, Webb et al. (2018, 2019) on the other hand recently showed that such hard power-law spectra are only achieved in relativistic shear flows, while the expected spectra become significantly softer for non-relativistic flow speeds. This Letter aims to explore and recapture this by means of a simple analysis.

The starting point is the standard momentum-space diffusion equation with spatial escape incorporated by means of a simple momentum-dependent particle escape term $f/\tau_{\rm esc}(p)$, i.e.,

$$\frac{\partial f}{\partial t} = \frac{1}{p^2}\frac{\partial}{\partial p}\left(p^2 D_p \frac{\partial f}{\partial p}\right) - \frac{f}{\tau_{\rm esc}}. \quad (1)$$

Here, D_p denotes the momentum-space shear diffusion coefficient given by (Rieger & Duffy 2006)

$$D_p = \Gamma p^2 \tau_s \propto p^{2+\alpha}, \quad (2)$$

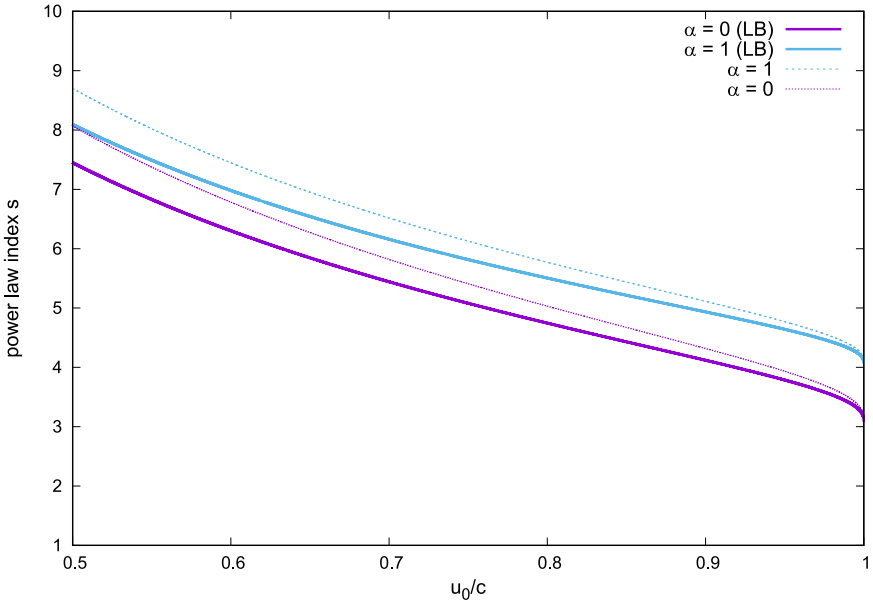

Figure 1. Power-law index s for the particle distribution $f(p) \propto p^{-s}$ as a function of the on-axis velocity u_0. A linearly decreasing velocity profile $u(r)$ with u_0 at r_0 and $u_2 = 0$ at r_2 has been assumed. The curves show the evolution in the assumed leaky-box (LB) approach for a scattering time $\tau_s \propto p^{\alpha}$ with $\alpha = 0$ and 1, respectively. For comparison, results of analytical solutions of the full particle transport equation are shown as thin (dotted and dashed) lines.

where $\tau_s(p)$ is the (momentum-dependent) mean scattering time assumed to follow a parameterization $\tau_s(p) = \tau_0\ (p/p_0)^{\alpha}$. Γ denotes the shear coefficient. For a simple shear flow velocity profile $\boldsymbol{u} = u_z(r)\boldsymbol{e}_z$, appropriate for a cylindrical outflow, one finds (Rieger & Duffy 2004; Webb et al. 2018)

$$\Gamma = \frac{1}{15}\,\gamma_b(r)^4\left(\frac{\partial u_z}{\partial r}\right)^2, \tag{3}$$

where $\gamma_b(r) = 1/(1 - u_z^2(r)/c^2)^{1/2}$. Following Equation (1) the characteristic (comoving) particle acceleration timescale can be expressed as (e.g., Rieger 2019)

$$t_{\rm acc}(p) = \frac{c}{(4+\alpha)\Gamma\,\lambda} \propto p^{-\alpha}, \tag{4}$$

where $\lambda(p) = \tau_s(p)c$ is the particle mean free path. The typical escape time, on the other hand, is determined by cross-field transport, i.e.,

$$\tau_{\rm esc}(p) \simeq \frac{(\Delta r)^2}{2\,\kappa(p)} \propto p^{-\alpha}, \tag{5}$$

where $\kappa(p) = \lambda(p)c/3$ is the spatial diffusion coefficient and Δr the width of the velocity shear region. Note that $t_{\rm acc}$ and $\tau_{\rm esc}$ have the same momentum dependence.

The approach in Equation (1) is somewhat analogous to the leaky-box model used to describe cosmic-ray (CR) transport in the Galaxy, in which spatial diffusion and convection are replaced by an escape term. In such models particles are considered to propagate freely with a small probability $(1/\tau_{\rm esc})$ of escape each time they reach the boundaries. The probability of a particle remaining in the box then is $\exp(-t/\tau_{\rm esc})$, and the particle distribution inside the containment region is uniform.

Looking for steady-state solutions of Equation (1) and employing a power-law Ansatz

$$f(p) = f_0\,p^{-s}, \tag{6}$$

the power-law index above injection p_0 is given by

$$s = \frac{(3+\alpha)}{2} + \sqrt{\frac{(3+\alpha)^2}{4} + (4+\alpha)\frac{t_{\rm acc}}{\tau_{\rm esc}}}. \tag{7}$$

Consequently, only for $t_{\rm acc} \ll \tau_{\rm esc}$, i.e., only for fast shear flows with $(\partial u_z/\partial r)(\Delta r) \to c$, is the power law $f(p) \propto p^{-(3+\alpha)}$ recovered, in which case the exponent only depends on the momentum dependence of the diffusion coefficient.

For illustration, consider a linearly decreasing velocity profile $u_z(r) = u_0 - (\Delta u_z/\Delta r)(r - r_0)$ with $\Delta u_z/\Delta r = (u_0 - u_2)/(r_2 - r_0)$, where the subscript 2 refers to quantities at the outer shear boundary, and where for the following we assume $u_2 = 0$ and $r_0 = 0$. Then, $(\partial u_z/\partial r) = (\Delta u_z/\Delta r)$, and formally

$$\frac{t_{\rm acc}}{\tau_{\rm esc}} = \frac{10}{(4+\alpha)\gamma_b(r)^4\left(\frac{\Delta u_z}{c}\right)^2}. \tag{8}$$

To treat the r-dependence in this expression, noting the second-order dependence on the velocity gradient, we replace $\gamma_b(r)^4$ by $\langle\gamma_b(r)^2\rangle^2$, where $\langle\rangle$ denotes averaging over r. This yields

$$s = \frac{(3+\alpha)}{2} + \sqrt{\frac{(3+\alpha)^2}{4} + 40\left(\ln\frac{(1+u_0/c)}{(1-u_0/c)}\right)^{-2}}. \tag{9}$$

The evolution of the power-law index s as a function of u_0 is shown in Figure 1. Obviously, for non-relativistic flow speeds u_0 the spectra can be much steeper, approaching the limiting value $s = (3+\alpha)$ only at relativistic speeds $u_0 \to c$. In Figure 1 we also show the evolution of the power-law index based on analytical solutions $f(r, p)$ of the full particle transport equation (Webb et al. 2018) for comparison. No one-to-one correspondence is expected, though, as a specific r-dependence of the scattering time $\tau_s(r,\ p)$ has been assumed in the derivation of these solutions (typically resulting in $\tau_s \to \infty$ as $r \to 0$), and as the leaky-box approach implies a simplified

treatment of spatial diffusion. Nevertheless, the qualitative behavior is reasonably well reproduced, deviations being at the ∼10% level. For $\gamma_b(r_0) = 4$ for example, one obtains $s = 3.6$ ($\alpha = 0$) and $s = 4.5$ ($\alpha = 1$), respectively. Note, however, that the expected power-law index s is in general sensitive to the employed velocity profile, with steeper shapes toward lower speeds being possible (e.g., Webb et al. 2019). However, this effect becomes less important in the relativistic limit and a more detailed analysis is left to a future paper.

The results shown here nicely illustrate that efficient shear acceleration requires relativistic velocity gradients. In principle, such velocity gradients appear to be possible in AGN, not only on smaller (sub-parsec) but also on larger (kiloparsec) jet scales, in particular in view of recent jet simulations showing that backflow speeds in AGN can be substantial (e.g., Perucho & Martí 2007; Rossi et al. 2008; Matthews et al. 2019; Perucho et al. 2019). We note that even for a less powerful FR I jet source such as M87, superluminal motion has been seen on kiloparsec scales (e.g., Meyer et al. 2017; Snios et al. 2019).

3. Maximum Energies

While experiencing shear acceleration, particles can also lose energy via synchrotron radiation on a characteristic (comoving) timescale $t_{\rm syn} = \frac{9m^3c^5}{4e^4\gamma B^2}$. This becomes particularly relevant for electrons. One can estimate achievable maximum energies ($\gamma_{\rm max}$) by equating the acceleration timescale (see Equation (4)) with the loss timescale. For simplicity we consider a quasi-linear-type parameterization for the particle mean free path (e.g., Liu et al. 2017) in the following, i.e.,

$$\lambda \simeq \xi^{-1} r_g \left(\frac{r_g}{\Lambda_{\rm max}}\right)^{1-q} \propto \gamma^{2-q}, \tag{10}$$

where $\xi \leqslant 1$ denotes the energy density ratio of turbulent versus regular magnetic field B, $\Lambda_{\rm max}$ is the longest interacting wavelength of the turbulence, r_g is the particle Larmor radius, γ is the particle Lorentz factor, and q is the power index of the turbulence spectrum (i.e., $q = 1$ for Bohm-type, $q = 3/2$ for Kraichnan-type, and $q = 5/3$ for Kolmogorov-type turbulence). In our notation, $\alpha = 2 - q$. Hence, for $0 < \alpha < 1$ we obtain

$$\gamma_{\rm max} = \left[\frac{9(4+\alpha)(mc^2)^{3+\alpha}(\Gamma/c^2)\,\Lambda_{\rm max}^{1-\alpha}}{4\,\xi\, e^{4+\alpha} B^{2+\alpha}}\right]^{\frac{1}{1-\alpha}}, \tag{11}$$

with $\gamma_{\rm max}$, γ and B measured in the comoving frame. For $\alpha > 1$, on the other hand, acceleration, once operative, proceeds faster than synchrotron cooling. For a Kolomogorov-type turbulence ($\alpha = 1/3$) and the linearly decreasing flow profile above with $\gamma_b(r_0) = 3$, $\xi = 0.2$ and $\Lambda_{\rm max} = \Delta r$, where Δr is the lateral width of the shear layer, Equation (11) evaluates to

$$\gamma_{e,\rm max} \simeq 3.5 \times 10^8 \left(\frac{30\,\mu{\rm G}}{B}\right)^{7/2} \left(\frac{0.1\ {\rm kpc}}{\Delta r}\right)^2, \tag{12}$$

suggesting that electron Lorentz factors $\gamma_e \sim (10^8$–$10^9)$ are in principle achievable in the large-scale jets of AGN. This would provide support to the electron synchrotron interpretation of extended X-ray emission in AGN jets that requires ultra-relativistic electrons be sustained along the jet (e.g., Harris & Krawczynski 2006; Georganopoulos et al. 2016). Note that for a Kraichnan-type turbulence ($\alpha = 1/2$), the numerical value, Equation (12), would be reduced by a factor of ∼20. In principle, due to the inverse dependence of $t_{\rm acc}$ on γ (Equation (4)) efficient electron acceleration typically requires the injection of energetic seed particles. The latter could, however, most likely be provided by conventional Fermi-type acceleration processes (Liu et al. 2017; Rieger 2019).

On the other hand, given their larger mean free path, shear acceleration of hadronic CRs is usually much easier to achieve. This could be of relevance for the origin of the highest-energy CRs. Current evidence suggests that the CR composition around 10^{18} eV is dominated by light primaries. Given the observed level of isotropy in arrival directions, these CRs have to be of extragalactic (possibly AGN-type) origin so as to avoid a large anisotropy toward the Galactic plane. With increasing energy the composition then seems to become more heavier ($\log(E_t[{\rm eV}]) = 18.3$ transition), with a trend that protons are gradually replaced by helium, helium by nitrogen, etc., an iron contribution possibly emerging above $\log(E[{\rm eV}]) = 19.4$ (e.g., see Alves Batista et al. 2019; Kachelriess & Semikoz 2019 for reviews).

To enable shear acceleration of cosmic-ray protons to energies E_t in the laboratory frame, corresponding to $E_t' = E_t/\gamma_b$ in the comoving frame, CR particles need to satisfy (see Liu et al. 2017; Webb et al. 2019) (i) the (lateral) confinement condition, $\lambda(E_t') \leqslant \Delta r$; (ii) the efficiency condition, $t_{\rm acc} \leqslant t_{\rm syn}$; and (iii) the longitudinal confinement constraint, $t_{\rm acc} \leqslant t_{\rm dyn} = d/(u_z\gamma_b)$, where d is the jet length, and $t_{\rm dyn}$, $t_{\rm acc}$, $t_{\rm syn}$ refer to the comoving frame. Figure 2 shows the parameter space (shear layer width Δr versus comoving magnetic field strength B) permitted by these constraints in the case of $\alpha = 1/3$ for the linearly decreasing shear flow profile above with $\gamma_b(r_0) = 3$. A jet shear width-to-length ratio $\rho_w = \Delta r/d = 0.02$, and $\xi = 1$ has been assumed in these calculations. For a magnetic field strength of 10^{-5} G, for example, a width $\gtrsim$0.1 kpc would be required. Such conditions are likely to be satisfied in the large-scale jets of AGN. Inspection of Figure 2 indicates that for a given jet width and magnetic field, the Hillas-type (Hillas 1984) confinement condition (i) usually imposes the tightest constraint on the maximum CR energy. This suggests that CR particles are able to reach

$$E_{\rm CR}' \simeq 3 \times 10^{18} Z\, \xi^{\frac{1}{\alpha}} \left(\frac{B}{30\,\mu{\rm G}}\right)\left(\frac{\Delta r}{0.1\ {\rm kpc}}\right) {\rm eV}, \tag{13}$$

where Z is the charge number. In the case of strong turbulence, $\xi \sim 1$, proton acceleration to E_t appears feasible, with the composition gradually becoming heavier. Note that due to the inverse scaling $t_{\rm acc} \propto 1/\lambda$ efficient injection may take place at different energy thresholds, and detailed modeling would be required to estimate the relative CR contribution at the highest energies. Pick-up shear acceleration of PeV CR protons (similar to our own Galaxy), however, is possible in the case of $\alpha = 1/3$ as $t_{\rm acc}/t_{\rm dyn} \simeq 2 \times 10^{-3}(100\ {\rm kpc}/d)$. The particle spectrum of CRs escaping the acceleration region approximately follows $\dot{n}_{\rm esc}(p) \propto p^2 f(p)/\tau_{\rm esc} \propto p^{2+\alpha-s}$, and can thus

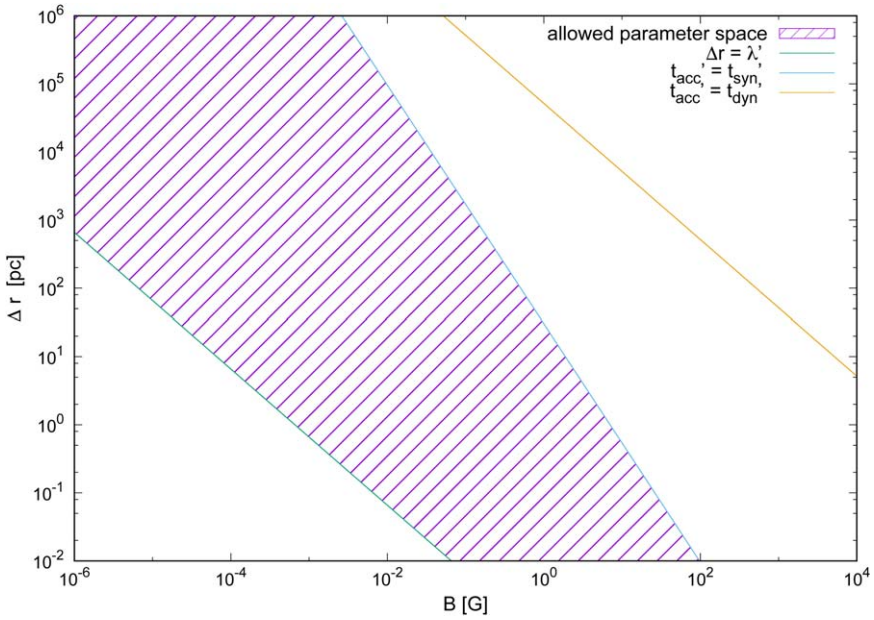

Figure 2. Allowed parameter range (shaded) for shear acceleration of CR protons to energies $E'_p = 10^{18}$ eV for a particle mean free path $\lambda' \propto p'^{\alpha}$ with $\alpha = 1/3$ (corresponding to Kolmogorov-type turbulence $q = 5/3$). A flow Lorentz factor $\gamma_b(r_0) = 3$ has been assumed.

be quite hard. We note that the present approach is complementary to the non-gradual ones discussed in Kimura et al. (2018) and Caprioli (2015), which are applicable for sufficiently narrow layers and ultra-fast ($\gamma_b \sim 30$) flow speeds, respectively (e.g., see Rieger 2019 for a discussion).

4. Conclusion

As shown here, fast shear flows can facilitate a continued Fermi-type acceleration of charged particles, capable of producing power-law particle momentum distributions as long as the velocity shear persists. In general, however, relativistic flow velocities are required for this mechanism to operate efficiently. As discussed here, such velocities may be encountered in the jets of AGN. Evaluating achievable electron energies (synchrotron-limited to PeV [10^{15} eV] energies) suggest that gradual shear acceleration could offer an interesting explanation for the extended high-energy emission observed in large-scale AGN jets. Similarly, EeV [10^{18} eV] energies (confinement-limited) may be achieved for cosmic-ray protons, indicating that shear acceleration in AGN jets could play a relevant role in the energization of the observed ultra-high-energy CRs. While these estimates are based on a simplified treatment and more extended studies are required, it seems hard to see how velocity shear could not play a role in the energization of charged particles.

F.M.R. kindly acknowledges funding by a DFG Heisenberg Fellowship RI 1187/6-1. Discussions with Gary Webb and Martin Lemoine are gratefully acknowledged. We thank the anonymous referee for insightful comments.

ORCID iDs

Frank M. Rieger https://orcid.org/0000-0003-1334-2993

References

Alves Batista, R., Biteau, J., Bustamante, M., et al. 2019, FrASS, 6, 23
Berezhko, E. G. 1982, SvAL, 8, 403
Berezhko, E. G., & Krymskii, G. F. 1981, SvAL, 7, 352
Blasi, M. G., Lico, R., Giroletti, M., et al. 2013, A&A, 559, A75
Boccardi, B., Krichbaum, T. P., Bach, U., et al. 2016, A&A, 585, A33
Caprioli, D. 2015, ApJL, 811, L38
Chhotray, A., Nappo, F., Ghisellini, G., et al. 2017, MNRAS, 466, 3544
Earl, J. A., Jokipii, J. R., & Morfill, G. 1988, ApJL, 331, L91
Fendt, C. 2019, Univ, 5, 99
Gabuzda, D. C., Reichstein, A. R., & O'Neill, E. L. 2014, MNRAS, 444, 172
Georganopoulos, M., Meyer, E., & Perlman, E. 2016, Galax, 4, 65
Giroletti, M., Giovannini, G., Cotton, W. D., et al. 2008, A&A, 488, 905
Harris, D. E., & Krawczynski, H. 2006, ARA&A, 44, 463
Hillas, A. M. 1984, ARA&A, 22, 425
Kachelriess, M., & Semikoz, D. V. 2019, PrPNP, 109, 103710
Kimura, S. S., Murase, K., & Zhang, B. T. 2018, PhRvD, 97, 023026
Laing, R. A., & Bridle, A. H. 2014, MNRAS, 437, 3405
Lemoine, M. 2019, PhRvD, 99, 083006
Liang, E., Fu, W., & Böttcher, M. 2017, ApJ, 847, 90
Liu, R.-Y., Rieger, F. M., & Aharonian, F. A. 2017, ApJ, 842, 39
Martí, J.-M. 2019, Galax, 7, 24
Matthews, J. H., Bell, A. R., Blundell, K. M., & Araudo, A. T. 2019, MNRAS, 482, 4303
Meyer, E., Sparks, W., Georganopoulos, M., et al. 2017, Galax, 5, 8
Nagai, H., Haga, T., Giovannini, G., et al. 2014, ApJ, 785, 53
Perucho, M. 2019, Galax, 7, 70
Perucho, M., & Martí, J. M. 2007, MNRAS, 382, 526
Perucho, M., Martí, J.-M., & Quilis, V. 2019, MNRAS, 482, 3718
Piner, B. G., & Edwards, P. G. 2014, ApJ, 797, 25
Rieger, F. M. 2019, Galax, 7, 78
Rieger, F. M., & Duffy, P. 2004, ApJ, 617, 155
Rieger, F. M., & Duffy, P. 2006, ApJ, 652, 1044
Rieger, F. M., & Duffy, P. 2016, ApJ, 833, 34
Rossi, P., Mignone, A., Bodo, G., Massaglia, S., & Ferrari, A. 2008, A&A, 488, 795
Sahayanathan, S. 2009, MNRAS, 398, L49
Snios, B., Nulsen, P. E. J., Kraft, R. P., et al. 2019, ApJ, 879, 8
Tavecchio, F., & Ghisellini, G. 2015, MNRAS, 451, 1502
Webb, G. M. 1989, ApJ, 340, 1112
Webb, G. M., Al-Nussirat, S., Mostafavi, P., et al. 2019, ApJ, 881, 123
Webb, G. M., Barghouty, A. F., Hu, Q., & le Roux, J. A. 2018, ApJ, 855, 31